Prevailing Features of X-Ray-Induced Molecular Electron Spectra Revealed with Fullerenes

Abraham Camacho Garibay, Ulf Saalmann, and Jan M. Rost
Max Planck Institute for the Physics of Complex Systems, Nöthnitzer Straße 38, 01187 Dresden, Germany
(Received 11 March 2014; published 18 August 2014)

X-ray photoabsorption from intense short pulses by a molecule triggers complicated electron and subsequently ion dynamics, leading to photoelectron spectra, which are difficult to interpret. Illuminating fullerenes offers a way to separate out the electron dynamics since the cage structure confines spatially the origin of photo- and Auger electrons. Together with the sequential nature of the photoprocesses at intensities available at x-ray free-electron lasers, this allows for a remarkably detailed interpretation of the photoelectron spectra, as we will demonstrate. The general features derived can serve as a paradigm for less well-defined situations in other large molecules or clusters.

DOI: 10.1103/PhysRevLett.113.083001 PACS numbers: 33.80.Wz, 41.60.Cr, 79.77.+g, 81.05.ub

Intense x-ray pulses from free-electron lasers [1,2] trigger multiple electron emission from a large molecule. The resulting electron spectrum is quite complex, containing photoelectrons (e_p), Auger electrons (e_a), and electrons evaporating from an almost thermalized nanoplasma cloud trapped by a positive background charge in the molecule, formed as a consequence of the electrons leaving the system [3–6]. This charge is considerably larger than in synchrotron experiments [7] and, along with the corresponding attractive potential, depends on time. The latter builds up quickly with the departure of e_p and e_a while it becomes weaker upon expansion induced by ion-ion repulsion. Charging and expansion of the ionic backbone crucially influence through this potential the electron spectrum since they determine the energy each individual electron carries after leaving the molecule; see Fig. 1.

In this situation, it is very desirable to analyze a molecule which exhibits all the features described yet offers a chance for simplification due to its symmetry. An ideal candidate is the C_{60} fullerene, which has 60 identical carbon atoms on a spherical shell such that each C atom has the same distance to the molecular center. Its electronic structure and dynamics have been probed in numerous studies by impact of electrons [8] or highly charged ions [9,10], and by synchrotrons [11] and intense femtosecond lasers [12,13]. Recent free-electron laser experiments have given intriguing x-ray diffraction data of crystalline C_{60} [14] as well as ion fragment spectra from free C_{60} [15], while electron spectra are yet to be addressed.

Here, we provide insight into the electron spectrum of C_{60} in the gas phase (similar to former studies with clusters [16]) through a theoretical approach which step by step adds complications to the dynamics of the fullerene, ultimately providing a realistic spectrum whose features become then understandable as remnants of the artificially simplified dynamics introduced before. To this end, we will first consider one e_p (and an accompanying e_a) per atom without trapping and plasma formation and discuss the different shapes of the spectrum obtained from rate equations as a function of the ratio of the Auger rate γ and photoionization rate κ. Of course, we keep all ions fixed for this synthetic spectrum. In a next step, we provide the full electron spectrum of C_{60} for multichannel ionization and Auger events determined by a molecular dynamics calculation but still for fixed ions. In a final step, we present full dynamical electron spectra, including ion motion, starting from very short but realistic pulses (1 fs duration, 10^{19} W/cm^2 intensity) to make contact with the fixed-ion spectra. We will see that ion motion significantly changes the spectra for longer pulses (up to 15 fs).

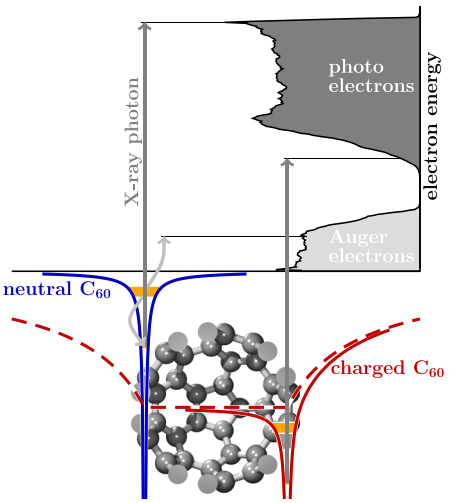

FIG. 1 (color online). Sketch of the formation of broad electron spectra. The highest energy is observed for the photoionization of core electrons from neutral C_{60} (solid blue line on the left). For a charged C_{60} (solid red line on the right), the energy is reduced due to the background potential (dashed red line).

 © 2014 American Physical Society

Photoabsorption as well as Auger-decay processes are modeled with a Monte Carlo procedure. We include all possible transitions (ss, sp, and pp) with branching ratios according to the atomic case [17] and the instantaneous valence-shell occupations [18]. Auger processes are described on the basis of a molecular Auger lifetime of 6 fs, a typical value for carbon in a molecular environment [19,20]. We restrict photoabsorption to the $1s$ carbon orbitals, which accounts for 95% of the total absorption of photons with energies larger than 1 keV [21]. Note that radiative decay (fluorescence) of carbon core holes in a molecular environment is about 2 orders of magnitude slower than nonradiative (Auger) decay [17].

The probability that an electron is emitted with energy E is given by an integral [22] over emission times $P(E) = \int dt p(t)\delta(E - E'(t))$, with $p(t)$ the ionization rate at time t and $E'(t)$ the final energy of an electron released at that time. The energy E' is time dependent due to the formation of a background potential mentioned before and given explicitly in Eq. (2). Considering various ionization channels x to be specified below, and writing the ionization rate in terms of $n(t)$, the number of electrons released up to time t, the spectrum reads

$$P(E) = \sum_x \int dt\, \dot{n}_x(t)\delta(E - E'_x(t)), \tag{1a}$$

$$= \sum_x \left| \frac{\dot{n}_x(t)}{\dot{E}'_x(t)} \right|_{t=t'_x(E)}, \tag{1b}$$

where $t'_x(E)$ is the inverse function of $E'_x(t)$ [22]. Time derivatives are denoted with a dot. The final energies of the electrons depend on the charge of all other ions in the C_{60} at the instant of their creation. Only for the simplest approach used in step I we do distribute the overall charge $Q(t)$ homogeneously over a sphere with radius $R(t)$. The corresponding potential is shown in Fig. 1 as a dashed line. Thereby, the final energies are

$$E_x(t) = E^\star_x + V(t), \tag{2a}$$

$$V(t) = -\frac{Q(t)}{R(t)}, \qquad Q(t) = \sum_x n_x(t), \tag{2b}$$

where $E^\star_x$ are the excess energies for an electron released from channel x of a single carbon atom. The excess energies appear as characteristic energies in the spectrum

$$E^\star_{\mathrm{ph}} = E_\omega - B_0, \tag{3a}$$

$$E^\star_{\mathrm{Auger}} = A_1, \tag{3b}$$

$$E^{\mathrm{min}}_{\mathrm{ph}} = E_\omega - B_{j_{\mathrm{max}}} - \tilde{Q}/R_0, \tag{3c}$$

with B_j the binding energies of the $1s$ core in C^{j+} and A_j the energies of the valence electrons released during the Auger decay α_j of a core-hole ion C^{j+}. Indeed, there are various Auger-decay channels with different energies for a certain charge state j. Since those differences are small on the energy scale considered here, we use in the discussion A_j as the average of those energies corresponding to α_j. The photo- and Auger excess energies [Eqs. (3a) and (3b)] are "upper limits" and correspond to the respective atomic carbon lines. The third energy [Eq. (3c)] marks a "lower limit." It is observed for the last e_p which is released from $C^{j_{\mathrm{max}}+}$ and an overall charge $\tilde{Q} = Q(t \to \infty)$. Here and in the following, we denote final variables with a tilde. As mentioned before, for the moment, we neglect ionic motion and set $R(t) = R_0 = 3.52$ Å.

We consider in our first simple step only one e_p per (fixed) atom in C_{60} and the subsequent e_a. This leads to the coupled rate equations for the time-dependent numbers of neutral atoms k and the singly and doubly charged ions k^+ and k^{++}:

$$\dot{k}(t) = -\kappa(t)k(t), \tag{4a}$$

$$\dot{k}^+(t) = \kappa(t)k(t) - \gamma k^+(t), \tag{4b}$$

$$\dot{k}^{++}(t) = \gamma k^+(t). \tag{4c}$$

The initial conditions ($t \to -\infty$) for neutral C_{60} are $k = 60$ and $k^+ = k^{++} = 0$. From the ion numbers follow the number of photoelectrons $\dot{n}_{\mathrm{ph}}(t) = -\dot{k}(t)$ and of Auger electrons $\dot{n}_{\mathrm{Auger}}(t) = \dot{k}^{++}(t)$.

To simplify things even more, we consider first a rectangular pulse with a constant κ, which allows an explicit solution of the rate equations (4). The resulting spectrum is shown in Fig. 2 for $E^\star_{\mathrm{ph}} = 500$ eV and various ratios κ/γ as colored regions. We have set $\gamma = 1$ and chosen κ accordingly. The pulse duration T was adapted in order to absorb 25 photons; i.e., for $t \to +\infty$, it is $\tilde{n}_{\mathrm{ph}} \approx 25$, and, of course, $\tilde{n}_{\mathrm{Auger}} = \tilde{n}_{\mathrm{ph}}$.

For very fast photoionization ($\kappa \to \infty$), all e_p produced by the laser pulse have escaped before the first e_a is emitted. Consequently, the last e_p has to escape against a potential of $\tilde{V} \approx -100$ eV, which results from the positive charge of $\tilde{Q} = \tilde{n}_{\mathrm{ph}}$ accumulated through photoionization. This explains the rectangular high-energy spectrum in Fig. 2(a). Such plateaulike spectra have been seen [23] and explained [23–25] before for the valence ionization of atomic clusters. Indeed, their appearance is quite general [6,26]. The final energy of the first e_a is reduced from $E^\star_{\mathrm{Auger}} = 250$ eV to $E^\star_{\mathrm{Auger}} - \tilde{V}$, while those of the last one is reduced by $2\tilde{V} \approx -200$ eV, since now the total positive charge is $\tilde{Q} = 2\tilde{n}_{\mathrm{ph}}$. This explains the low-energy rectangular spectrum for energies $E = 50, \ldots, 150$ eV.

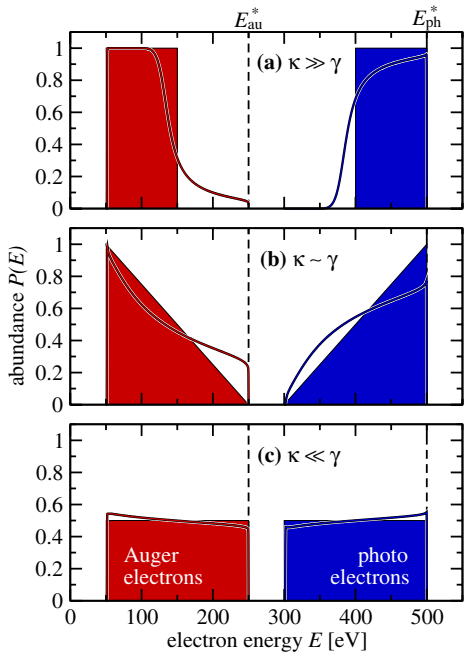

FIG. 2 (color online). Spectra for photo- (blue) and Auger (red) electrons for three scenarios (a)–(c) corresponding to different ratios of the photoionization rate κ to the Auger rate ($\gamma = 1$). The solid lines show the result for Gaussian pulses: from top to bottom, $\bar{\kappa}/\gamma = 10, 1, 1/10$ with pulse durations $T = 2/\bar{\kappa} = 2/10$, 2, 20, respectively. Shaded areas mark the results for rectangular pulses, in (a) and (c) for the limiting cases $\kappa \to \infty$ and $\gamma \to \infty$, respectively, and in (b) for the special case of a fixed ratio $\kappa/\gamma = 2$. The atomic excess energies of $E^\star_{\text{Auger}} = 250$ eV and $E^\star_{\text{ph}} = 500$ eV are marked by dashed lines.

For the spectrum in Fig. 2(c), the Auger decays are instantaneous ($\gamma \gg \kappa$), implying that in between two photoionization events, an Auger event takes place. Therefore, the background charge for the next e_p increases by $\delta Q = 2$, stretching the interval of the photoelectron spectrum by a factor of 2 to energies $E = 300, \ldots, 500$ eV. The same is true for the Auger spectrum since each photoelectron is accompanied by an Auger electron. The overall shift of about 250 eV is due to a lower excess energy $E^\star_{\text{Auger}}$.

Flat spectra emerge if photoionization and Auger decay are decoupled due to very different rates. This changes if both rates are similar. In particular, for $\kappa/\gamma = 2$, the electron spectrum takes a triangular form, as shown in Fig. 2(b). This shape can be obtained analytically from Eq. (1). The spectra with a time-dependent photoionization rate $\kappa(t) = \bar{\kappa}\sqrt{6/\pi}\exp[-(t/T)^2]$ following a realistic Gaussian pulse can be understood as deviations from the idealized shapes just discussed for constant photoabsorption in the three limiting cases of κ/γ ratios; see Figs. 2(a)–2(c). Here, we compare the mean photoionization rate $\bar{\kappa}$ [27] with the Auger rate γ.

As a next step of complication, we discuss the full electron spectrum for fixed ions resulting from many-channel electron dynamics including double core-hole and plasma formation for the scenarios (a) and (b) from Fig. 2. Results have been obtained by propagating the released electrons by means of molecular dynamics in the potential of the increasingly charged C_{60}, which, due to the creation of core holes at different sites, is not spherical as in Eq. (2). Photon frequency ($E_\omega = 2$ keV) and intensity are chosen such that more than 200 photoelectrons are produced to activate all subsequent channels down to photoionization of the ground state of C^{5+} with $B_5 = 476$ eV entering Eq. (3c). Besides, this choice assures us that spectral regions of e_p and e_a do not overlap.

In scenario (b), the photoionization rate is small enough that, on average, an e_a is produced after each e_p. A characteristic step appears at energy $E_{\text{trap}} = E_\omega - B_0 - A_1 = 1476$ eV [see Fig. 3(b)] separating the high-energy part from the low-energy part in the photoelectron spectrum. In the former, after each e_p, an e_a escapes, increasing the background charge by $\delta Q = 2$, while in the latter, the e_a is trapped such that $\delta Q = 1$. Trapping occurs if the background potential is deep enough such that $Q_{\text{trap}}/R = A_1 = 239$ eV, the kinetic energy of the e_a produced in the Auger decay of C^+ with a $1s$ hole. Consequently, $Q_{\text{trap}}/2 \approx 29$ is the number of escaped e_a, provided this step at E_{trap} exists in the spectrum. With the 29 escaped e_a and the $238 e_p$, we estimate from Eq. (3c) $E^{\text{min}}_{\text{ph}} = 440$ eV, in good agreement with Fig. 3(b).

The spectrum of scenario (a) with $\kappa \gg \gamma$ lacks E_{trap}, since fast photoionization builds up a large Q before e_a are produced. Dominant photoionization early in the pulse is confirmed by the triangular shape of the e_p spectrum at its blue edge ($E \lesssim E^\star_{\text{ph}}$). It forms if exactly two channels contribute whose rate has the ratio 2. This is the case for photoionization of C and C^+ with a single core hole without significant influence of other channels, e.g., Auger escape. Given that situation, we can read off from

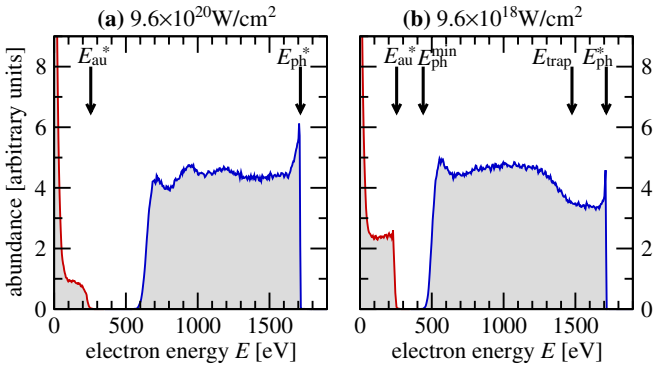

FIG. 3 (color online). Electron spectra for fixed ions generated with an x-ray pulse of 2 keV photons. The peak intensities are 9.6×10^{20} and 9.6×10^{18} W/cm^2 for scenarios (a) and (b), respectively. From the area under the e_p spectrum in the interval $[E^{\text{min}}_{\text{ph}}, E^\star_{\text{ph}}]$ follows the number of e_p: $n^{(b)}_{\text{ph}} = 238$ and $n^{(a)}_{\text{ph}} = 217$.

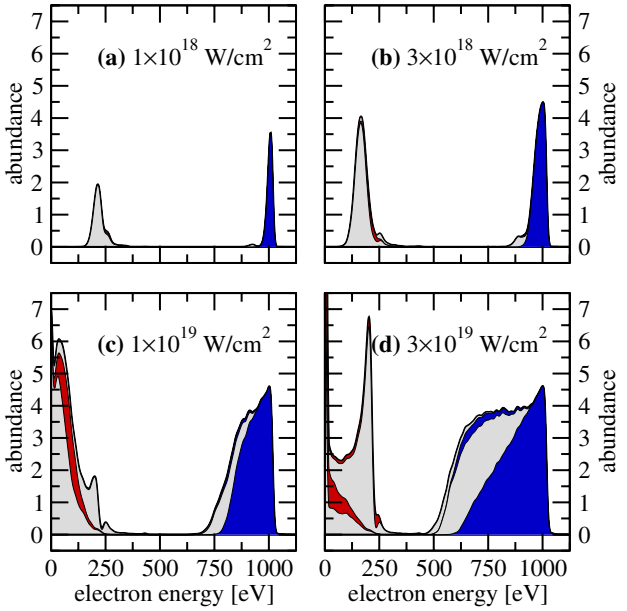

FIG. 4 (color online). (a)–(d) Electron energy spectra from C_{60} exposed to a short pulse ($T = 1$ fs) of $E_\omega = 1.3$ keV photons for various intensities with Auger and photoelectrons are below or above 400 eV, respectively. In order to highlight contributions from different channels, even channels (ionization of C^{2j+}) are colored red and blue, respectively, and odd channels ($C^{(2j+1)+}$) are colored gray. The area under the photoelectron spectra provides the numbers of photoelectrons: $\{n_{\rm ph}^{(a)}, n_{\rm ph}^{(b)}, n_{\rm ph}^{(c)}, n_{\rm ph}^{(d)}\} = \{6, 17, 48, 98\}$.

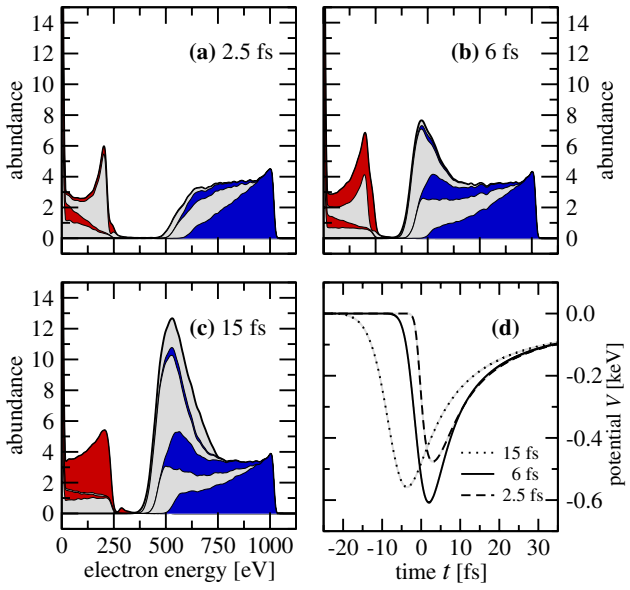

FIG. 5 (color online). (a)–(c) Electron energy spectra as in Fig. 4 (same color coding) but for a fixed peak intensity of $I = 10^{19}$ W/cm^2 and various pulse lengths T. Note that the spectrum for $T = 1$ fs with the same intensity I is shown in Fig. 4(c). (d) The time-dependent background potential $V(t)$, given by Eq. (2b), for the same pulse parameters. The numbers of photoelectrons are $\{n_{\rm ph}^{(a)}, n_{\rm ph}^{(b)}, n_{\rm ph}^{(c)}, n_{\rm ph}^{(d)}\} = \{48, 96, 155, 208\}$.

Fig. 3(a) that $E_{\rm ph}^{\rm min} \approx 600$ eV and estimate with the help of Eq. (3c) and the $217e_p$ that about $10e_a$ have escaped.

We are now in a position to understand the truly complex electron spectra resulting from full electron and ion dynamics when illuminated by an intense x-ray pulse of $E_\omega = 1.3$ keV photons, which is sufficient to retain a spectral gap between photo- and Auger electrons. The highest intensities used are realistic, assuming 10^{13} photons per pulse focused onto 1 μm^2, which gives roughly $I_{\rm max} \approx (2/T_{\rm fs}) \times 10^{20}$ W/cm^2. To make contact with the frozen ions discussed so far, we consider first in Fig. 4 a $T = 1$ fs pulse. For weak intensity, i.e., only a few electrons ionized, the spectrum in Fig. 4(a) shows peaks slightly redshifted to the atomic photoelectron and Auger-electron energies $E_{\rm ph}^\star$ and $E_{\rm Auger}^\star$. For further increasing intensity, the familiar *plateau* for the e_p develops due to the generation of background charge Q, and for the same reason, the Auger peak gets an increasing redshift. As in Fig. 3, the energies $E_{\rm ph}^{\rm min}$ are consistent with the number of e_p and e_a which have escaped and the relevant excess energies B_j; see the caption of Fig. 3. However, the e_a reveal a new feature, namely, the reappearance of a peak close to the atomic line $A_3 = 224$ eV for high intensity; see Figs. 4(c) and 4(d). The reason for this behavior is that the background potential [Eq. (2b)] is weak at early *and* at late times when the fullerene is either weakly charged ($Q \approx 0$) or is exploded ($R \to \infty$); see Fig. 5(d). Indeed, further analysis reveals that the α_3-related peaks in Figs. 4(c) and 4(d) require a preceding Auger decay α_2 due to the short pulse (1 fs) which considerably delays the α_3 decay.

The nonmonotonic time dependence of the background potential together with the different emission times of the electrons can qualitatively change the shape of the electron spectra. This is further corroborated with Figs. 5(a)–5(c), also revealing drastic changes in the photoelectron spectrum for longer pulses. Electrons emitted late in or even after the laser pulse lose less and less energy, turning the formation of a plateau into a pileup of electrons in a small energy interval, particularly striking for the (late) photoelectrons from C^{j+} with $j > 2$ in Fig. 5(c).

In summary, we have analyzed the electron spectra of fullerenes following irradiation of short and intense x-ray pulses. These spectra reveal general features which will also allow one to interpret spectra of less symmetric large molecules. First, triangular shapes will appear whenever two ionization channels are dominant, with one twice as likely as the other, as it is the case with the photoionization of a filled ($1s^2$) and half filled ($1s$) core shell, indicating double core-hole formation. Second, we have established the onset $E_{\rm ph}^{\rm min}$ of the e_p spectrum as characteristic energy which allows one to determine directly the number of escaped e_a. Third, from electrons emitted late in or after the pulse, a peak at the blue edge of the Auger spectrum and at the red edge of the photoelectron spectrum will appear for

long enough laser pulses due to the time dependence of the background potential. Since this is a general and robust mechanism, we also expect those peaks in less symmetric molecules.

This work was supported by the COST Action XLIC (CM 1204) and the Marie Curie Initial Training Network CORINF.

[1] H. Chapman, J. Ullrich, and J. M. Rost, J. Phys. B **43**, 190201 (2010).
[2] P. Bucksbaum, T. Möller, and K. Ueda, J. Phys. B **46**, 160201 (2013).
[3] U. Saalmann and J. M. Rost, Phys. Rev. Lett. **89**, 143401 (2002).
[4] B. Ziaja, T. Laarmann, H. Wabnitz, F. Wang, E. Weckert, C. Bostedt, and T. Möller, New J. Phys. **11**, 103012 (2009).
[5] C. Bostedt, H. Thomas, M. Hoener, T. Möller, U. Saalmann, I. Georgescu, C. Gnodtke, and J.-M. Rost, New J. Phys. **12**, 083004 (2010).
[6] M. Arbeiter and T. Fennel, New J. Phys. **13**, 053022 (2011).
[7] R. C. Bilodeau *et al.*, Phys. Rev. Lett. **111**, 043003 (2013).
[8] R. Völpel, G. Hofmann, M. Steidl, M. Stenke, M. Schlapp, R. Trassl, and E. Salzborn, Phys. Rev. Lett. **71**, 3439 (1993).
[9] H. Cederquist *et al.*, Phys. Rev. A **61**, 022712 (2000).
[10] H. Cederquist, J. Jensen, H. Schmidt, H. Zettergren, S. Tomita, B. A. Huber, and B. Manil, Phys. Rev. A **67**, 062719 (2003).
[11] S. W. J. Scully *et al.*, Phys. Rev. Lett. **94**, 065503 (2005).
[12] E. E. B. Campbell, K. Hansen, K. Hoffmann, G. Korn, M. Tchaplyguine, M. Wittmann, and I. Hertel, Phys. Rev. Lett. **84**, 2128 (2000).
[13] I. V. Hertel, I. Shchatsinin, T. Laarmann, N. Zhavoronkov, H.-H. Ritze, and C. P. Schulz, Phys. Rev. Lett. **102**, 023003 (2009).
[14] B. Abbey *et al.*, arXiv:1209.5168.
[15] B. F. Murphy *et al.*, Nat. Commun. **5**, 4281 (2014).
[16] C. Bostedt, M. Adolph, E. Eremina, M. Hoener, D. Rupp, S. Schorb, H. Thomas, A. R. B. de Castro, and T. Möller, J. Phys. B **43**, 194011 (2010); U. Saalmann, J. Phys. B **43**, 194012 (2010).
[17] E. Hartmann, J. Phys. B **21**, 1173 (1988).
[18] P. Di Cintio, U. Saalmann, and J.-M. Rost, Phys. Rev. Lett. **111**, 123401 (2013).
[19] T. X. Carroll, J. Hahne, T. Thomas, L. Sæthre, N. Berrah, J. Bozek, and E. Kukk, Phys. Rev. A **61**, 042503 (2000).
[20] A. S. Schlachter *et al.*, J. Phys. B **37**, L103 (2004).
[21] J. J. Yeh and I. Lindau, At. Data Nucl. Data Tables **32**, 1 (1985).
[22] J. M. Rost, Phys. Rep. **297**, 271 (1998).
[23] C. Bostedt *et al.*, Phys. Rev. Lett. **100**, 133401 (2008).
[24] M. Arbeiter and T. Fennel, Phys. Rev. A **82**, 013201 (2010).
[25] C. Gnodtke, U. Saalmann, and J.-M. Rost, New J. Phys. **13**, 013028 (2011); Chem. Phys. **414**, 65 (2013).
[26] K. Moribayashi, Phys. Rev. A **80**, 025403 (2009).
[27] The mean photoionization rate is defined by requiring that the zeroth and second moments $\int dt\,\kappa(t)$ and $\int dt\,t^2\kappa(t)$, respectively, agree with the corresponding values for a rectangular pulse with a fixed photoionization rate $\bar{\kappa}\,\bar{T}$ and $\bar{\kappa}\bar{T}^3/12$, respectively.